SUPPLEMENTARY INFORMATION

1. Materials and methods.

Fabrication of microfluidic devices. We fabricated polycarbonate chips in 5-mm thick plates (Macroclear, Bayer, Germany) using a CNC milling machine (MSG4025, Ergwind, Poland). The milled plates were thermally bonded to flat 2-mm plates by compressing them together (30 min, 130 °C). We created the world-to-device interface using 21 gauge needles (~ 4 cm, O.D. 0.82 mm, I.D. 0.65 mm, Fishman Corporation, USA). We connected the device inlets to resistive steel capillaries (O.D. 400 μm, I.D. 205 μm, length 200 cm, Mifam, Poland) extending from the valves using short segments of Tygon® tubing (~ 2 cm, O.D. 0.91 mm, I.D. 0.25 mm, Ismatec, Switzerland) to connect the capillaries with the needles.

Automation and microfluidics. Custom written Lab View script controlled 13 valves (V165, equipped with Z070D coils, Sirai, Italy) via a National Instruments (USA) card (NI PCIE-6321). The valves controlled the flow of oil (n-hexadecane, Alfa Aesar, Germany) containing 0.4% (w/w) surfactant (Span80, Sigma Aldrich, Germany) from pressurized reservoirs, through the valves and into the steel capillaries and onto the chip. All aqueous samples were deposited on the chip into long storage channels directly from sterile syringes. Once the liquids were deposited on the chip, the flow of oil pushed the samples into the on-chip microdroplet generators. We controlled the pressure applied to the oil reservoirs using manual pressure regulators (Bosch Rexroth PR1-RGP, Germany) and monitored the pressure using digital manometers (AZ 82100, AZ Instruments, Taiwan). Generation of droplets was aided with an edge-detection algorithm to track the process of microdroplet formation and controlled the volume to an accuracy of ~0.3%. Merging of droplets was facilitated by using an electrocoalescence mechanism[1,2].

The chip contained waveguides (UM22-400, Thorlabs, USA) positioned perpendicularly to the direction of the incubation segment that enabled us to record light passing through the droplet with the OceanOptics USB2000+ spectrophotometer. We acquired full spectra at 500 Hz using an optical path (through the droplet) of 5 mm. To monitor the cell density in the microdroplet chemostats, we recorded absorbance at λ=600 nm. The high speed of measurements using the spectrophotometer made it possible for us to measure at least 70 spectra for each droplet as it flowed through the optical path, yielding 0.2% variability in measurements of optical density of microchemostats. A plot depicting the calibration is shown in Figure S5.

Antibiotics and bacteria. We prepared antibiotic stocks of chloramphenicol (Roth, Germany) immediately prior to experiments using 50% (v/v) aqueous solution of ethanol. The concentration of chloramphenicol was 1000x larger than the concentrations in the microchemostats. We sterilized antibiotic stock solution by filtration. Before each experiment, we diluted antibiotic stocks in LBK broth to the desired concentration and transferred the samples to the inlets of the device. The concentration of antibiotic was subsequently adjusted during the merging of droplets on-chip.

We used Luria-Bertani Broth (LB, BD Biosciences, Belgium) or its modified buffered version, LBK[3] in most experiments. LBK consists of 0.5% (w/v) yeast extract (BD Biosciences, Belgium), 1% (w/v) tryptone (BD Biosciences, Belgium), 0.64% potassium chloride (Sigma-Aldrich, Germany) and 100 mM of PIPES buffer (Sigma-Aldrich, Germany). We adjusted LBK broth to pH=7 using a 1 M solution of potassium hydroxide and subsequently sterilized the medium by filtration. As a model organism we used *E. coli* strain ATCC 25992. We prepared stock solution of cells in LB broth containing 30% glycerol (Chempur, Poland) and froze the stocks at -80 °C. Before performing experiments, we streaked cells on LB agar plates and incubated them overnight. We picked individual colonies, used them to inoculate liquid LBK broth, cultured cells at 37 °C and 200 rpm overnight, and transferred aliquots to fresh LBK media and grew them until the absorbance of 0.1 at λ=600 nm. We diluted the culture 10x in fresh medium prior to transferring suspensions of *E. coli* into microfluidic device. The only exception was in the experiments depicted in Figure S11 in which the microdroplets were not buffered the growth rate of bacteria was decreased.

2. Technical description of the experimental system.

Microdroplet chemostat design. The design of the microdroplet chemostat is shown in Fig. S1a. The system consists of:

- Electronic valve drivers (1 - Fig. S1a), which are controlled by a NI PCIE-6321 card on a PC. Their construction enables users to generate rectangular pulses which control the bi-stable coils (Z070D, Sirai, Italy). The high state of pulses corresponds to an open valve, while the low state of represents a closed valve.
- Oil containers (2 - Fig. S1a) are pressurized by an outer compressor using a manual pressure regulator.
- A set of capillaries and tubes transport oil (3 - Fig.S1a) from the containers to the chip. Controlled influx of the oil on a chip enables iterative operations on droplets circulating on a chip and subsequent removal of saturated culture medium. We plan to equip the system with a sample collector consisting of a microwell plate on an XY table. The motion of the table can be controlled using stepper motors directly from the NI PCIE-6321card.
- A thermostat (c - Fig. S1a) made using Styrofoam.
- A set of valves (Fig. S1b) enables users to turn on/off the flow in appropriate channels. In our system valves are connected to the chip via steel capillaries. The use of steel capillaries of high fluidic resistance allows for precise control of the flow on the chip and conducting iterative operations, including: change of the direction of flow, generation of droplets on demand, splitting droplets with an arbitrarily set ratio of split volumes, and merging with fresh aliquots of liquid.
- uEye camera (4 - Fig. S1c) operates on-line. Images are immediately processed using custom-coded software to trigger the valves.[4] For example, optical feedback enables us to produce monodisperse droplets regardless of the

changing hydraulic resistance on the chip. Droplets are diluted with continuous phase only when they achieve the desired (preprogrammed) length. The camera is focused only on a central part of the chip where droplets are formed, split and merged.

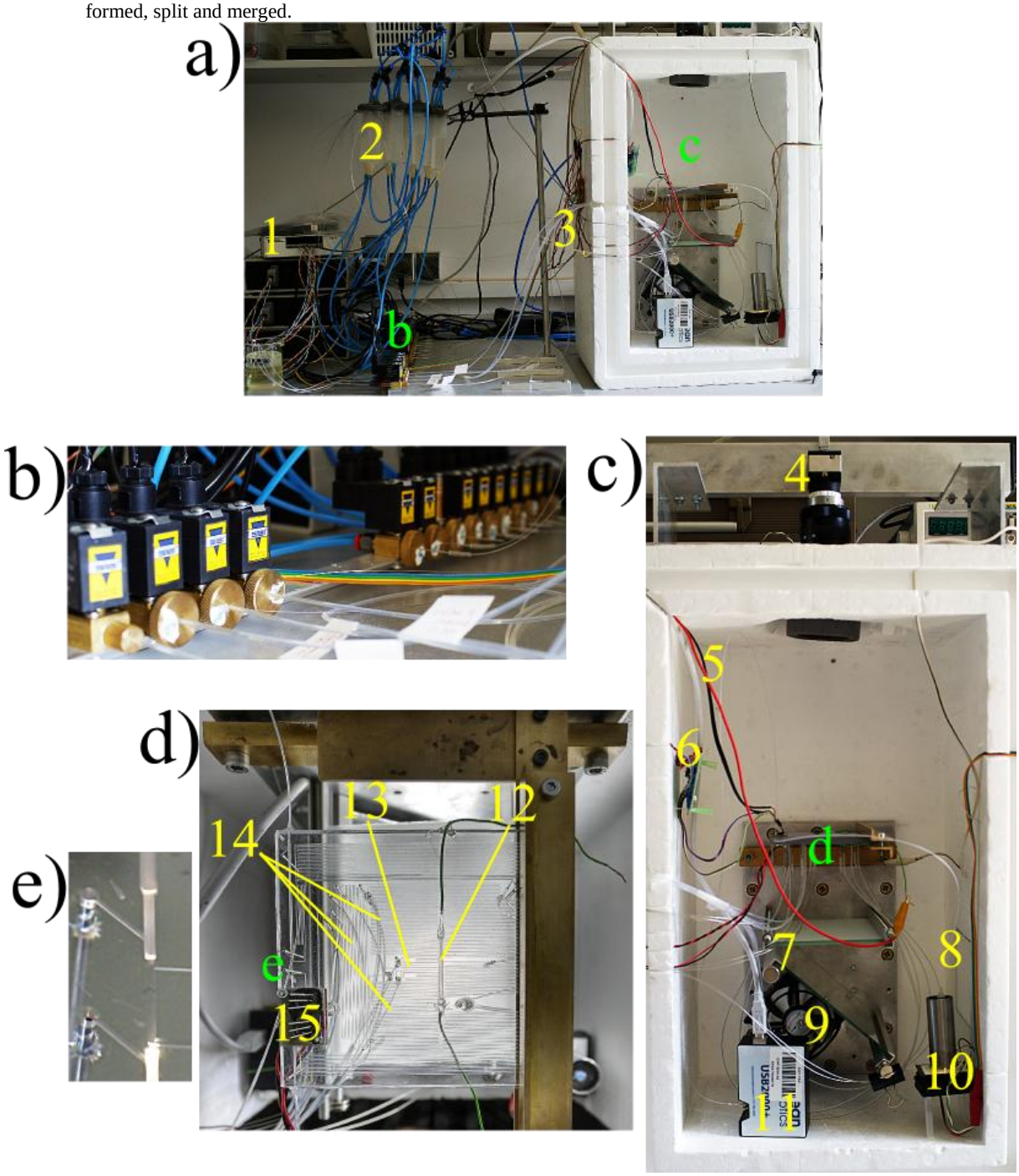

Figure S1. Photographs of the experiment: **a** - the whole setup including the thermostat enclosing the chip, the external valves, fluidic connections and the electronics, **b** - the set of valves, **c** - the thermostat, **d** – the microfluidic chip (top-down view), **e** – the location of waveguides for measuring OD.

- Wires providing high voltage enable the electrocoalescence of droplets (5 - Fig.S1c).
- An electronic module checks the volume of droplets and the distance between them (6 - Fig.S1c). The module consists of light-to-voltage converters (TSL257, TAOS), LED diodes, and digital electronics and generates appropriate triggering signal to the PC. Signal was correlated with the appearance of droplets at the defined place. The whole subsystem allows us to keep the distance between droplets and to measure the volumes of flowing droplets.
- A glass diffuser (7 - Fig.S1c) homogeneously illuminated the entire chip.

- A source of white light (8 - Fig.S1c) – the set of 81 white light LEDs (OF-SMD5060NW-H, OPTOFLASH) – is installed outside the isolated box and eliminates heat generated inside the box. The light passes through the isolating glass (8 - Fig.S1c) and glances off the mirror (placed at a 45^{o} angle) directly to the diffusive glass.
- A cooler and a heating plate are positioned at the back side of the temperature-stabilized box (9-Fig. S1c). The source of heat is based on a simple self-stabilization electronic component. The concept is to stabilize the current between the potentiometer, which sets the temperature, and a thyristor. The approach enables us to keep the temperature constant inside the box within a tenth of 1 °C. The cooler helps dissipate the heat from steel plate and provides stable temperature conditions inside the box.
- A reference light spectrophotometer (10 – Fig. S1c) provides a stable light intensity. We use a high-power LED (3W, SSCAN3220, Seoul Semiconductor) and checked that the fluctuation of light intensity was around 0.1 % of the set value over 48 h of operation.
- An Ocean Optics spectrophotometer (11 - Fig. S1c) enabled us to measure optical density in flowing droplets in a chip in real time at a frequency of 500 Hz. The long-term fluctuations of the signal from the spectrophotometer inside the temperature-stabilized box had standard deviation of ~0.0035 OD. We tried to eliminate the perturbation that the fluctuations had on our measurements by generating droplets during each exchange of the droplet volume (containing pure growth medium) at the beginning and the end of the sequence of droplets. This procedure enabled us to measure the reference intensity during each step of the experiment—notwithstanding the disturbance of our spectrophotometer and reference light—to an accuracy within 0.9% OD. This accuracy was also checked on the sequence of droplets containing varied concentrations of fluorescein (Fig. S2). We measured the intensity of fluorescence in real time in a chip placed on the stage of a confocal microscope over 48 h. The results of this crosscheck control experiment suggest limited (negligible) levels of the exchange of fluorescein between the droplets, and excluded drift in the sensitivity of the Ocean Optics spectrophotometer.
- The chip (Fig. S1d) was placed in the middle of the styrofoam box. Fig. S1d illustrates the chip with: i) the region where electrocoalescence is performed (12 – Fig. S1d) by applying an AC electric field (500V/mm, 200Hz); ii) three T-junctions (13-Fig. S1d) responsible for formation of droplets; iii) three areas with channels (14 - Fig. S1d), so-called “aspiration channels”, where the analytes are deposited[5] ; iv) the measurement region (15 – Fig. S1d) whether the electronic module measures the droplet volume and the distance between them; and v) the location of fiber optics (Fig. S1e), which enabled us to measure optical density of bacteria inside droplets in real time.

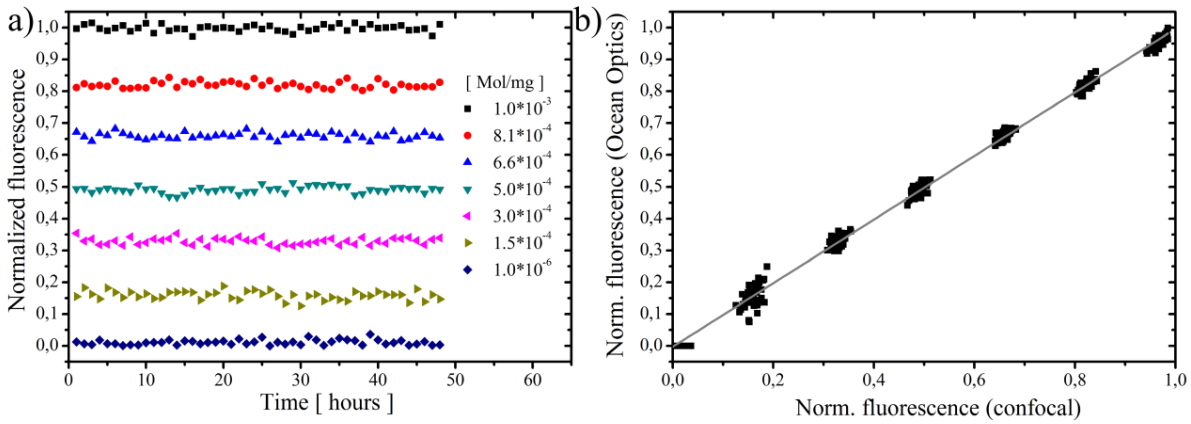

Figure S2. (a) A plot illustrating the measurement of the fluorescence intensity from a series of seven droplets containing varied concentrations of fluorescein. The 1.28 µL volume droplets had a center-to-center distance of 1 cm and were cycled back-and-forth in the microchannel with the same conditions used as in the microchemostat droplets experiments. No change in the level of fluorescence was observed during the experiment. **(b)** A plot depicting the correlation of the level fluorescence between measurements performed with the Ocean Optics spectrophotometer and with a Nikon A1R-A1 confocal microscope.

2. Accuracy of splitting droplets.

At user-defined intervals the microdroplet chemostats were split into two daughter droplets: a waste droplet and a seed droplet. The waste fraction was removed through the side channel and the seed microdroplet remained in the main channel. We were able to control the volume of the seed microdroplet between 0.1 - 0.9 of the volume of the initial microdroplet with an accuracy of ~0.8%. We merged the seed microdroplet with microdroplets containing reagents using an electrocoalescence mechanism (Supplementary Information, Video S2).

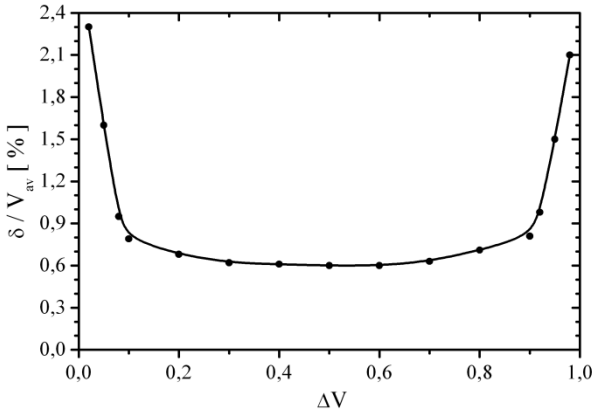

Figure S3. The maximum recorded error of the seed volume divided by the averaged seed volume as a function of the seed volume, normalized by the initial volume of the micro-chemostat.

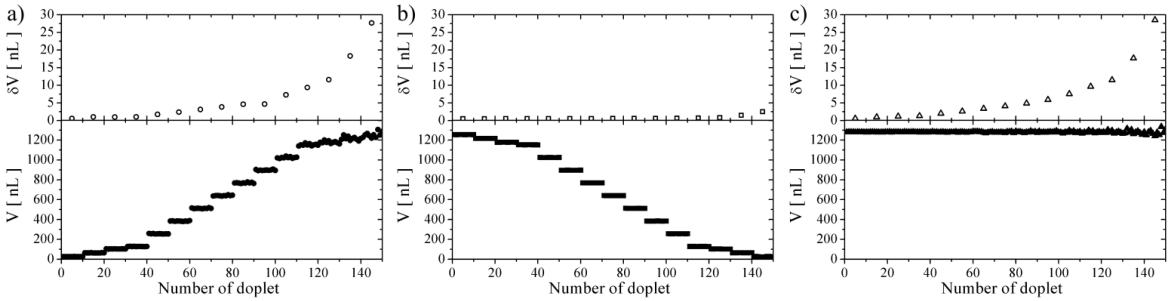

Figure S4. The plots depict the data used to plot Fig. S3. We performed 150 experiments that entailed splitting the chemostat microdroplets into a waste and seed droplets and subsequently merging he seed microdroplets with fresh media. Each nominal split ratio was repeated 10 times, yielding 15 groups of 10 measurements. The plot show the individual recordings of the volume in the bottom panels and the standard deviation calculated for the 10 measurements in the upper panels. **(a)** The waste droplets, **(b)** seed droplets, **(c)** droplets after merging with fresh media.

3. Calibration of the measurement of optical density.

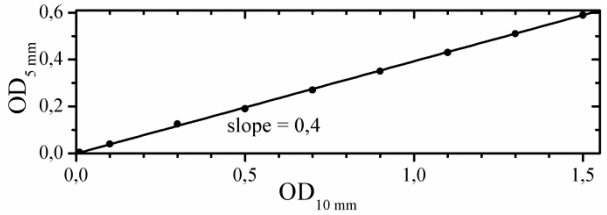

Figure S5. To characterize cell growth in microdroplets, we created a dilution series of cells in culture tubes (off-chip) and in microdroplets on-chip, and measured the absorbance of the suspension of cells at λ=600 nm in the microfluidic system (for microdroplets) and using a bench-top spectrophotometer (for tube cultures). The linear correlation between the two data sets enabled us to reliably estimate the number of cells (CFU) in microdroplets over time. The graph shows linear correlation between the absorbance at 600 nm recorded on-chip with the microdroplets over an optical length of L=5 mm, with the absorbance recorded on a standard spectrophotometer (L=10 mm) on the same suspensions of bacteria.

4. Changing concentration of soluble chemical factors in microdroplets in time.

We used solutions of red and blue dye to characterize the accuracy and reproducibility of systematic changes in chemical concentration within a lineage of microdroplets (Figure S6). We started with a microdroplet containing a mixture of red and blue dye. At each iteration we split the microdroplet and merged the seed droplet with a microdroplet containing a preprogrammed composition of dyes. This process changed the concentration of each dye independently. Figure S6 shows the absorbance of a microdroplet at λ=450 and at 650 nm, which corresponds to the concentration of blue and red dye, respectively. The largest root mean square error between the measured and programmed dye concentration was 0.7%. The value of the Pearson correlation for the two sets of measured and programmed concentrations was 0.996, which reflects a high accuracy in controlling the chemical composition of the lineage of the microdroplets in time.

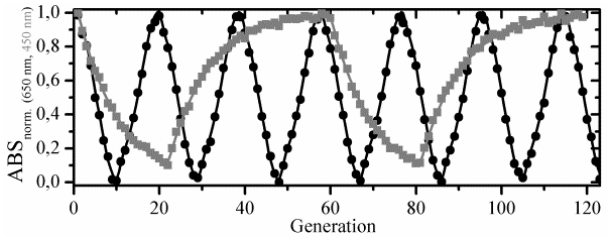

Figure S6. Graph of the normalized absorbance at 450 and 650 nm, showing exemplary traces of the concentration of blue and red dyes in a chemostat droplet over 120 generations. The data points show the measurements while the lines reflect the programmed values.

5. Density of cells in microchemostats.

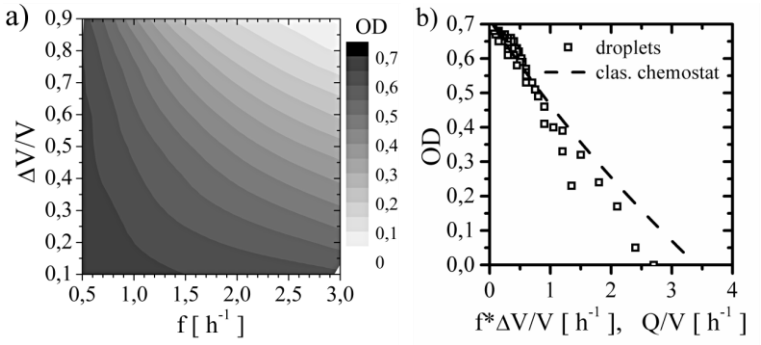

Figure S7. (a) A heat map illustrating the bacterial cell density at the moment of exchange of media as a function of the frequency of exchanges and the fraction of the volume of liquid exchanged. **(b)** A graph comparing the saturation density of cells at the moment of exchange to the density of cells in a chemostat with continuous exchange of media. "Droplets" refers to microdroplet chemostats; "Clas. Chemostat" refers to classical chemostats.

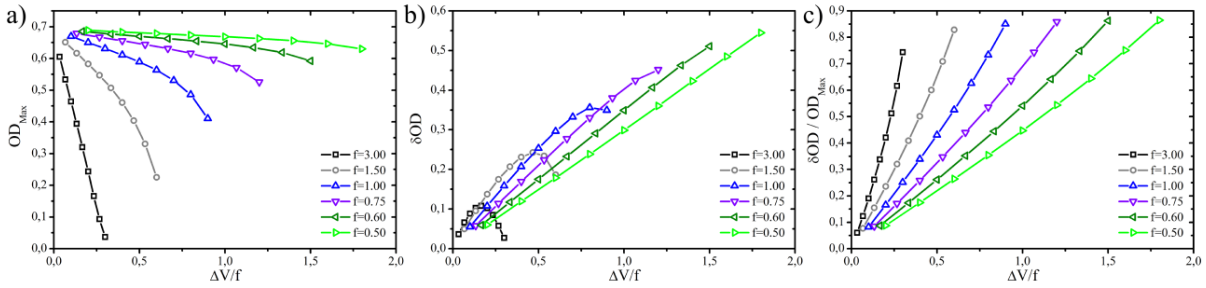

Figure S8. A set of plots depicting **(a)** the dependence of maximum optical density prior to exchanging the nutrient media as a function of the fraction of the exchanged volume divided by the frequency of exchanges, **(b)** the change of OD upon exchange of media, **(c)** normalized change of OD.

6. Dynamic stability of microchemostats as a function of errors in administering liquids.

To determine how errors in splitting/fusing of microdroplets propagate into fluctuations of cell density, we performed numerical simulations of Monod's equation using the experimentally determined parameters. We found that the standard deviation σ_N calculated for the density of cells at the moment of subsequent exchanges increased with the standard deviation σ_V of the exchange of volume (Figure S9). In our experiments σ_V is less than 1% of ΔV, i.e. in the range that does not lead to amplification of errors. This measurement agrees with the experimental observation that the value of N_{SAT} is stable over multiple iterations of growth and exchange of media.

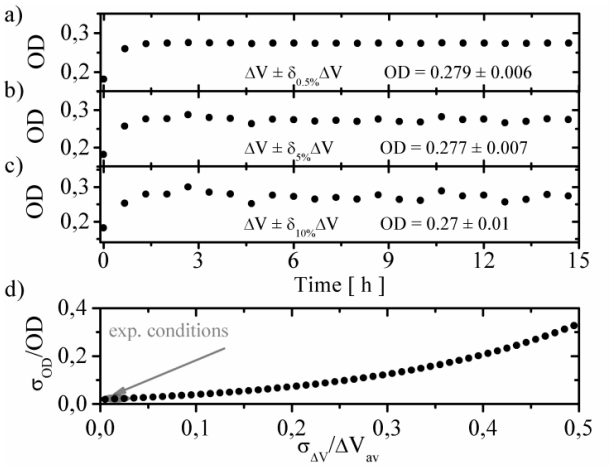

Figure S9. Results of numerical simulations. Figure S9 a-c) shows the deviations in the stabilization of optical density numerically simulated for three different perturbations (a, 0.5%; b, 5%; c, 10%) of the split volume of microdroplets. Figure S9 d) shows the dependence of the standard optical density deviation error divided by the averaged optical density on the standard volume deviation divided by the averaged split volume. The grey area indicates the conditions in our experiment. All calculations were based on the growth curves measured in our experiment (Figure 3a). We used an interval time between exchanges of 40 min. ($f = 1.5\ h^{-1}$) and an exchange volume of $\Delta V = 0.5$ for the microdroplets.

In a control experiment we prepared a sequence of 15 microdroplets containing 5 groups of 3 microdroplets with increasing concentration of chloroamphenicol (0.25, 0.55 and 1.1 µL/mg). The microdroplets contained *E. coli* cells at a concentration of $1.09 \pm 0.13 \times 10^7$ cfu/mL. We grew the cells in the microchemostats and calculated the standard deviation of the absorbance measured from the 5 microdroplets containing the same concentration of the drug at each exchange of the media. We obtained the values of 3.7% (for 0.25 µL/mg), 4.3% (0.55 µL/mg) and 5.7% (for 1.1 µL/mg) throughout a 50-hour experiment.

7. Experiments that verify the lack of cross-contamination between the microdroplet chemostats.

We have previously demonstrated that incubation of bacteria with antibiotic in microdroplets separated by hexadecane oil containing 2% Span 80 does not result in cross-contamination after several hours[1]. As the system presented allows for long-term incubation of microorganisms we performed additional long-term control experiments in which we compared the growth rate and saturation density of cells in adjacent microdroplets that either contained LBK nutrient media or LBK admixed with chlormamphenicol (10 µg/mL) and did not observe any cross-contamination.

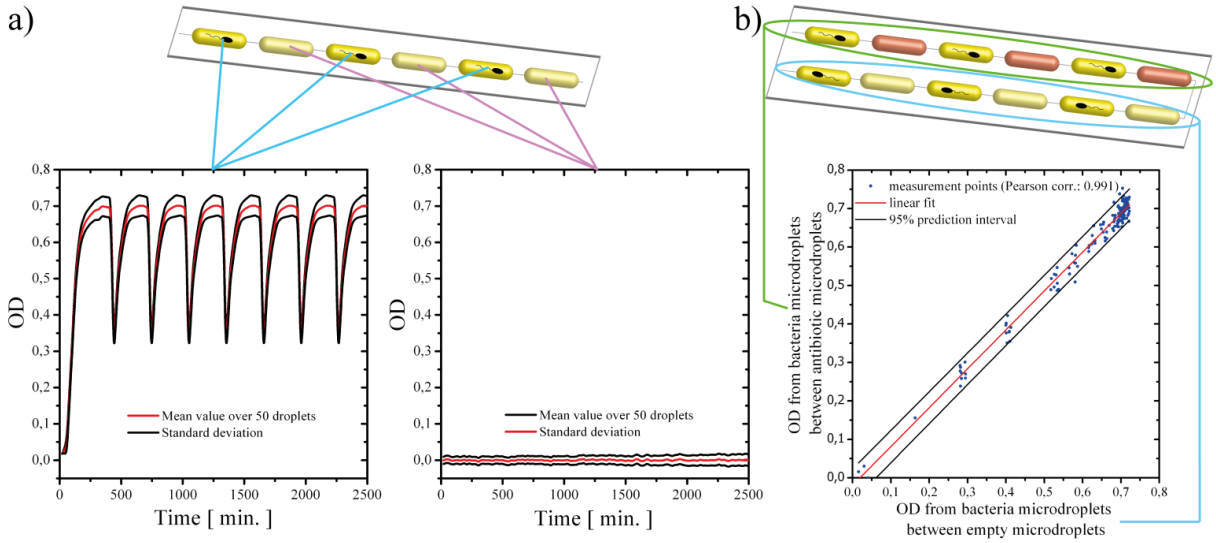

Figure S10. Results of experiments that demonstrate that there is no cross-contamination between the microdroplets in our system. **(a)** We prepared 100 microdroplets consisting of an alternating sequence of microdroplets seeded with bacteria and microdroplets only containing growth media. We did not observe cell growth in microdroplets that were initially free of cells. **(b)** In parallel we performed an experiment in which microdroplets containing bacteria were neighbouring in the sequence with microdroplets containing a highly concentrated solution of chloramphenicol (10 µg/mL). We incubated both sequences of microdroplets for 24 h at 37 °C and carried out 24 liquid exchange steps. We found a high correlation of bacteiral growth in the two experiments which thereby excluded the possibility of transfer of cells or antibiotics between microdroplets.

8. Growth-curves as a function of concentration of antibiotic

We determined the growth curves of ATCC 25992 strain as a function of the concentration of chloramphenicol in the LB medium. We prepared a sequence of 33 droplets, containing a range of concentrations of chloramphenicol (from 0.0 µg/mL to 1.0 µg/mL, with 0.1 µg/mL step size), with 3 microdroplets at each concentration. We ran the chemostat system for 10 h and measured the density of cells in microdroplets over time. Growth curves are illustrated in Figure S11. Measuring entire growth curves for each microdroplet enabled us to fit the data to Monod's equation, extract parameters, and quantitatively determine how the concentration of antibiotic influenced the growth rate (Figure S11 inset plot). This approach provides a quantitative method of determining the influence of soluble factors and inhibitors on the growth of cells in a population of bacteria.

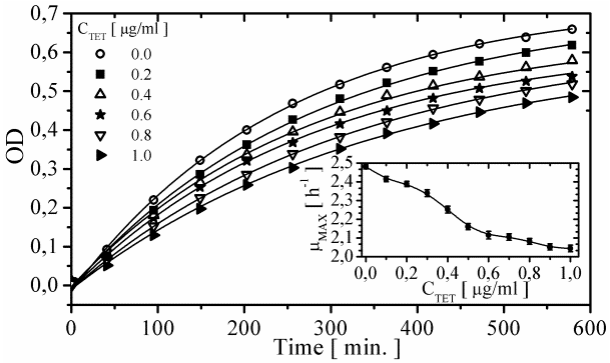

Figure S11. A plot depicting the growth of *E. coli* ATCC 25992 in the presence of various concentrations of tetracycline (0 to 1.0 µg/ml). For clarity, we only include representative curves for 6 concentrations. The inset plot illustrates the maximum growth rate as a function of antibiotic concentration.

9. Experiments with a varied ramp of the applied antibiotic stress.

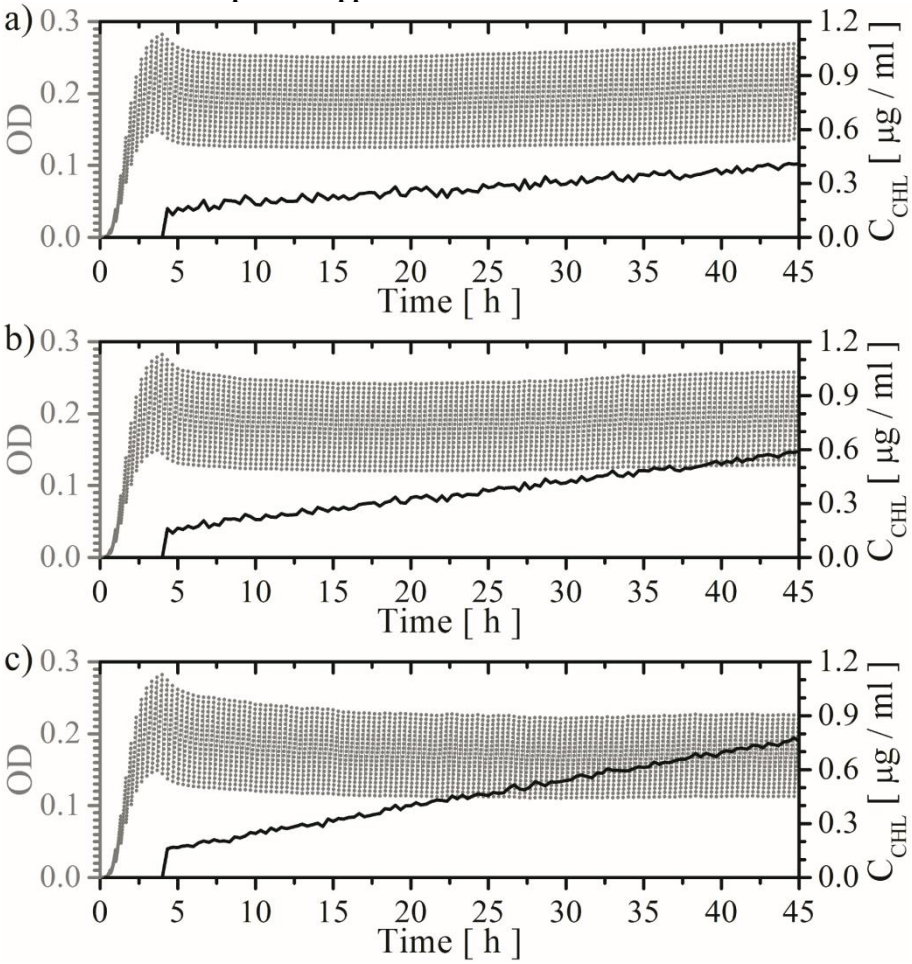

Figure S12. These plots demonstrate the change of growth curves of populations of *E. coli* in microchemostats and their response to slowly increasing levels of applied stress (i.e., antibiotics). We screened three rates of increasing the concentration of chloramphenicol: **(a)** 0.006 $\mu g \cdot mL^{-1} \cdot h^{-1}$; **(b)** 0.010 $\mu g \cdot mL^{-1} \cdot h^{-1}$; and **(c)** 0.015 $\mu g \cdot mL^{-1} \cdot h^{-1}$).

References

[1] K. Churski, P. Korczyk, P. Garstecki, Lab on a Chip **2010**, *10*, 816–818.

[2] T. Szymborski, P. M. Korczyk, R. Holyst, P. Garstecki, Applied Physics Letters **2011**, *99*, 094101-3.

[3] D. Blankenhorn, J. Phillips, J. L. Slonczewski, Journal of Bacteriology **1999**, *181*, 2209–2216.

[4] J. Guzowski, P.M. Korczyk, S. Jakiela, P. Garstecki, Lab on a Chip **2011**, *11*, 3593-3595.

[5] K. Churski, T.S. Kaminski, S. Jakiela, W. Kamysz, W. Baranska-Rybak, D. B. Weibel, P. Garstecki, Lab on a Chip **2012**, *12*, 1629-1637.